ENERGY STORAGE MANUFACTURING SCIENCE

Received March 25, 2026
Accepted April 15, 2026
DOI: 10.66655/sn7f4p84

A Guide from Laboratory Jet Milling as an Enabling Step in Sustainable All-Dry Manufacturing of Battery Materials

Fadilullahi Ayodeji Adeniyi[1#], Vadim Shipitsyn[1#], Chanmonirath (Michael) Chak[1], Yusheng Yan[1], Lin Ma[1]*

[1] Department of Applied Physical Sciences, The University of North Carolina at Chapel Hill, Chapel Hill, NC 27514, USA

[#] These authors contributed equally to this work.

*Author to whom any correspondence should be addressed.

Email: l.ma@unc.edu

Abstract

Lithium-ion battery (LIB) cathodes such as $LiNi_xMn_yCo_{1-x-y}O_2$ (NMC) and $LiFePO_4$ (LFP) dominate the market, yet conventional synthesis relies on water and energy intensive aqueous processes. All-dry manufacturing eliminates these issues, with jet milling (fluid-energy milling) enabling effective deagglomeration of sintered single-crystal NMC particles into discrete ~3 μm primaries with minimal contamination or damage. This study provides a detailed guide to laboratory-scale jet milling, covering equipment design, basic principles, and operation protocols (with supplementary instructional video). Using all-dry synthesized $LiNi_{0.5}Mn_{0.3}Co_{0.2}O_2$ (NMC532) as a case study, we demonstrate that optimal grinding pressure (120 psi) and feed rate (0.1–1.5 g min^{-1}) produce uniform, and narrow particle size distributions even after reheating step. We also provide an outlook on additional potential applications of jet milling in battery material processing. These advancements support the sustainable energy transition amid surging global battery demand.

Introduction

Lithium-ion batteries (LIBs) are essential for global electrification, powering critical applications such as artificial intelligence (AI) data centers, drones, and electrical grids[1,2] Consequently, the manufacturing demand for LIBs is projected to increase dramatically in the coming years. Cathode manufacturing is one of the most critical and resource-intensive stages in LIB production, as cathode materials largely govern battery energy density, voltage, safety, and cost[3].

$LiNi_xMn_yCo_{1-x-y}O_2$ (NMC) and lithium iron phosphate ($LiFePO_4$, LFP) represent the two mainstream cathode chemistries dominating the current market. However, conventional manufacturing routes for these materials are highly water and energy intensive[4,5]. NMC cathodes are typically synthesized by high-temperature sintering of a lithium source with transition metal (TM) hydroxide precursors[3].

The aqueous co-precipitation process used to produce these TM hydroxide precursors consumes vast quantities of water, often thousands of cubic meters per day at industrial scale for reaction, washing, and filtration, followed by energy-intensive drying steps prior to lithiation and sintering. Traditional LFP production primarily relies on solid-state or carbothermal reduction methods[3,6.] These routes frequently involve wet precipitation of iron phosphate precursors, followed by aqueous ball or sand milling with lithium and carbon sources, spray drying of the resulting slurry, and high-temperature sintering under inert atmosphere. This leads to substantial water consumption during precursor synthesis and mixing stages, along with high energy demands for drying and thermal processing.

All-dry manufacturing methods for cathode materials have emerged as a highly promising strategy to overcome these sustainability challenges by eliminating aqueous processing entirely. Recent demonstrations of all-dry processing for single-crystal NMC materials, yielding primary particles of approximately 3 μm with excellent mechanical properties and compatibility with elemental doping, have proven the technical feasibility and scalability of this approach[4,7,8].

A pivotal enabler of this success is the jet-milling technique (also known as fluid-energy milling). This dry comminution method employs high-pressure gas jets (typically compressed air or nitrogen) to accelerate particles within a grinding chamber, generating high-velocity particle–particle and particle–wall collisions that achieve precise size reduction and de-agglomeration with minimal contamination or heat generation. Jet milling is widely used across industries, including pharmaceuticals

(for active-ingredient micronization), food, chemicals, and advanced materials[9–12].

In LIB cathode manufacturing, jet milling is particularly effective for de-agglomerating sintered single crystal NMC particles, delivering discrete, well-separated primary single crystals without compromising crystal integrity[4,13]. Despite its central importance, this straightforward yet powerful tool has only been mentioned cursorily in previous studies on all-dry cathode processing[4,13], with little detail provided on equipment construction, working mechanisms, calibration, or operational protocols for the broader research community.

To address this gap, the present work utilizes a laboratory-scale jet mill to provide a comprehensive introduction to this technology. We describe the instrument's construction, fundamental working mechanisms, and detailed operation protocols, accompanied by a supplementary instructional video. Using the processing of single-crystal $LiNi_{0.5}Mn_{0.3}Co_{0.2}O_2$ (NMC532) as a representative case study, we systematically investigated the influence of two key operational parameters, grinding gas pressure and feed rate, on the final particle-size distribution of the product. We also discuss the broader potential applications of jet milling in LFP cathode manufacturing, surface coating and beyond lithium materials processing.

Experimental

Material Synthesis. NMC532 was synthesized by an all-dry solid-state route. Nickel(II) carbonate anhydrous ($NiCO_3$; Thermo Scientific, 98%), manganese(IV) oxide (MnO_2; Thermo Scientific, 99.9%), and cobalt(II,III) oxide (Co_3O_4; Thermo Scientific, 99.7%) were used as TM precursors, and lithium carbonate (Li_2CO_3; Thermo Scientific, >99%) served as the lithium source. All reagents were used as received.

An initial 0.5 g batch of NMC532 was prepared using stoichiometric quantities corresponding to a Ni:Mn:Co molar ratio of 5:3:2. Lithium carbonate was added to provide a Li/TM molar ratio of 1.20 to compensate for lithium volatilization during high-temperature calcination. The precursor powders were manually homogenized in an agate mortar and pestle for approximately 30 min to promote uniform solid–solid mixing. The blended powder was transferred to an alumina crucible and calcined in air in a muffle furnace (KSL-1100X, MTI Corporation) using a heating ramp of 5 °C min^{-1} to 950 °C, held for 10 h, and allowed to cool naturally inside the furnace.

These conditions yielded single-phase layered NMC532 and were adopted for subsequent larger-scale synthesis used in the jet milling studies. After jet milling (described below), selected samples were reheated at 750 °C for 3 h in the air.

Powder X-ray diffraction (XRD). Powder XRD was performed using a Rigaku SmartLab diffractometer (Japan). Diffraction data were collected using Cu Kα radiation over an appropriate 2θ range. **Scanning electron microscopy (SEM).** Particle morphology was examined using a Hitachi S-4700 cold cathode field emission SEM (Japan) operating in secondary electron mode. Powders were dispersed onto conductive carbon tape to minimize charging. Micrographs were collected at 20.0 kV accelerating voltage with a working distance of approximately 11.7 mm. **Energy-dispersive X-ray spectroscopy (EDS).** Elemental composition and spatial distribution were analyzed using an Oxford Instruments INCA PentaFET-x3 system integrated with the SEM. Measurements were conducted at 20.0 kV to ensure excitation of transition-metal characteristic X-ray lines. **Particle size distribution (PSD).** Particle size analysis was performed from SEM micrographs using ImageJ software. Representative images acquired at ×1,000 and ×3,000 magnifications were used for measurement. Individual particles were manually measured using the line measurement tool, and diameters were determined based on projected particle size. A statistically meaningful number of particles were analyzed for each sample to ensure representative distributions. The collected measurements were exported and processed in Origin software to generate particle size distribution curves.

Jet Milling Procedure. Jet milling was performed using a laboratory-scale fluid-energy mill (Glen Mills, Model "00" JET-O-MIZER, USA). A photograph of the complete milling assembly is shown in **Figure S1**, and labeled internal components are provided. Nitrogen gas supplied from a compressed cylinder was regulated prior to entering the system in this study. Internal operating pressures were controlled using the instrument regulators including supply gas valve, pusher nozzle, and grinding nozzles (**Figure S1**). Prior to systematic experiments, the vibratory feeder (Syntron) was calibrated to establish reproducible powder delivery. A baseline feed rate of 1.5 g min^{-1} was achieved by distributing powder uniformly along approximately 26 cm of the V-shaped trough and operating the vibrator at a setting of 3. Integrated operation delivered 1 g of powder in approximately 45 s. Lower and higher feed rates (0.1 and 50 g min^{-1}) were obtained by adjusting vibrator intensity while maintaining consistent powder distribution length. Operational procedures for start-up, steady-state milling, shutdown, and cleaning followed manufacturer guidelines. Particular attention was given to airtight connections, confirmation of suction at the feed inlet, and coordinated control of pusher and grinding nozzles to prevent backflow or hopper kickback. The mill was cleaned between experiments to avoid cross-contamination. A detailed visual demonstration of assembly, calibration, operation, and troubleshooting procedures is provided in the supplementary instructional video accompanying this work.

Results and Discussion

The core component of the jet milling system is the milling chamber (**Figure 1a-b**). In the jet mill employed in this study, the chamber is vertically oriented, with multiple tangential grinding nozzles positioned at the base as shown by the purple arrow in **Figure 1b**. High-pressure gas is introduced through these nozzles, creating high-velocity jets that enter tangentially and generate a strong upward-spiraling vortex and circulating flow within the chamber as shown by the orange arrow in **Figure 1b**. Particles follow a helical trajectory in this vortex, undergoing repeated cycles. Particle size reduction occurs primarily through high-energy interparticle collisions in the high-velocity spiral flow path.

The milling chamber features a tapered (conical) design, which concentrates particles near the nozzle region to promote intense collisions and enhance grinding efficiency. Finer particles are entrained by the ascending gas flow and exit centrally through the top (**Figure 1b**), while coarser particles remain in the circulating loop for further size reduction.

Raw powder or granules are fed into the milling chamber via an inlet located on the top right side of the chamber (indicated by the red arrow in **Figure 1b**). This feed inlet connects to a hopper (**Figure 1b**) containing the raw material. The powder/granules are entrained by a small flow of high-pressure gas supplied through a dedicated "feed gas" line (controlled by the pusher nozzle), sourced from the same compressed gas system as the grinding nozzles. This feed gas accelerates through a narrowing (Venturi-type) nozzle, creating suction that draws material from the hopper and injects it directly into the intense grinding vortex.

The suction mechanism relies on the Venturi effect, governed by Bernoulli's principle:

$$\frac{v^2}{2} + gz + \frac{p}{\rho} = constant$$

where:

v is the fluid flow speed at a point,

g is the acceleration due to gravity,

z is the elevation of the point above a reference plane,

p is the static pressure at the chosen point, and

ρ is the density of the fluid at all points in the fluid.

As the high-pressure feed gas is forced through the constricted nozzle, its velocity increases dramatically, resulting in a corresponding decrease in static pressure in the mixing zone (below atmospheric pressure). This low-pressure region generates sufficient suction to draw atmospheric air and entrain the powder/granules from the hopper into the high-velocity gas stream. Once entrained, particles are rapidly accelerated by the main grinding jets and undergo high-speed interparticle collisions.

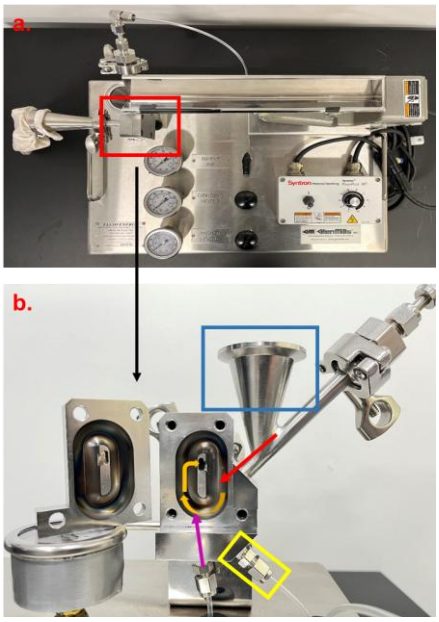

Figure 1. A laboratory-scale fluid-energy (jet) mill used in this study. (a) Full view of the equipment, with the red square highlighting the milling chamber. (b) Detailed view of the milling chamber. The blue square indicates the hopper containing the raw powder/granules. The yellow square marks the connection to the pusher nozzle pressure gauge (no visible inlet hole in this view), which monitors the feed gas pressure driving material injection. The red arrow denotes the direction of material entrainment from the pusher nozzle into the milling chamber (via the inlet hole). The purple arrows indicate the tangential entry directions of high-pressure gas from the grinding nozzles (two small orifices visible), which generate the high-velocity jets for particle-on-particle collisions in the vortex as shown by the orange arrow.

The system offers flexibility in gas type (e.g., air, nitrogen) and is readily scalable for larger throughput. Key operating parameters include grinding pressure (which controls jet velocity and collision energy) and feed rate (which influences particle concentration and residence time in the grinding zone). In the following case study, we demonstrate the influence of these parameters during the processing of NMC532 cathode material.

NMC532 cathode material was synthesized via a one-pot all-dry method by sintering a stoichiometric mixture of precursors at 950 °C for 10 h in air. XRD confirmed the formation of a single-phase layered structure (**Figure 2a**). EDS mapping revealed homogeneous distribution of Ni, Mn, and Co throughout the particles (**Figure 2b–c**). However, the as-sintered material exhibited significant agglomeration, with clusters composed of primary single crystal particles formed during high-temperature sintering (**Figure 2d**). Deagglomeration via jet milling is essential in this all-dry synthesis route. It disperses the clusters into

discrete single crystal primary particles (typically ~3 µm in size), enabling true single crystal morphology by minimizing grain boundaries. This reduces intergranular cracking, enhances structural stability during electrochemical cycling, and promotes uniform particle size distribution[7,14]. Deagglomerated particles also pack more densely, improving tap density and volumetric energy density in fabricated electrodes.

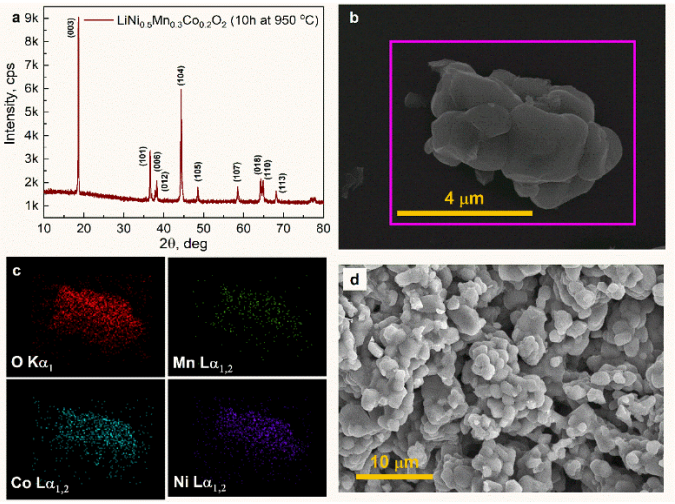

Figure 2. Characterization of NMC532 cathode material synthesized via one-pot all-dry method by sintering at 950 °C for 10 h in air. (a) Powder XRD pattern confirming single-phase layered structure. (b) SEM image of agglomerated particle region. (c) Corresponding EDS elemental maps showing homogeneous distribution of Ni, Mn, and Co. (d) Additional SEM image of the as-synthesized material morphology.

The effect of grinding nozzle pressure on particle characteristics was investigated first (**Figure 3**, **Table S1**). Three pressures were evaluated: 10 psi, 60 psi, and 120 psi. The starting material was the agglomerated NMC532 sintered at 950 °C for 10 h (as shown in **Figure 2**). Increasing grinding pressure progressively reduced particle size and narrowed the particle size distribution, indicating improved homogeneity (**Figure 3a–d, 3i-k**). At 120 psi, well-dispersed single-crystal particles were clearly observed via SEM. Following jet milling, all samples were re-heated at 750 °C for 3 h in air to reduce surface impurities and heal any defects introduced during milling, as re-heating is a critical step in all-dry synthesis for restoring pristine surface chemistry[4,13]. Jet milling is a dry comminution process that relies on high velocity particle–particle collisions and therefore does not chemically introduce external contaminants. However, increasing the specific surface area and generating fresh fractured facets can temporarily enhance the reactivity of layered NMC toward atmospheric H_2O and CO_2. Numerous reports have shown that Ni-rich and mid-Ni NMC compositions readily form LiOH, Li_2CO_3, and metal hydroxide/carboxylate phases upon ambient exposure[15–17]. Such surface layers can therefore accumulate more readily after jet milling due to the creation of reactive surface terminations.

The subsequent reheating step serves to remove these adventitious species. Recent all-dry processing work demonstrated that jet milling increases surface residual lithium content and that reheating at 750 °C for 3 h effectively reduces Li_2CO_3 and related lithium containing species to levels comparable to commercial materials, while preserving single crystal morphology and without inducing additional cation mixing[4].Thus, although jet milling could temporarily promote adsorption of atmospheric species, reheating efficiently eliminates these surface impurities and restores a clean, stable surface structure in the final product.

Post-re-heating, morphology and particle size distribution remained largely unchanged for the 60 psi and 120 psi samples, while the 10 psi sample exhibited a broader particle size distribution (**Figure 3e–h, 3l-n**), suggesting insufficient deagglomeration at lower pressure.

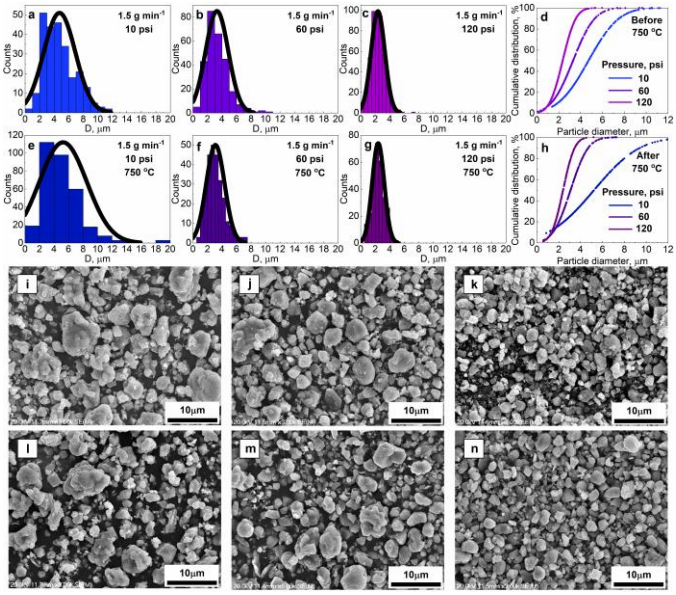

Figure 3. Particle size distributions of NMC532 cathode material determined from statistical SEM image analysis, showing the effect of grinding pressure in jet milling. (a–d) As-sintered NMC532 (one-pot all-dry synthesis at 950 °C for 10 h in air): histograms of particle counts vs. diameter at grinding pressures of (a) 10 psi, (b) 60 psi, and (c) 120 psi; (d) corresponding cumulative distribution curves (percentage vs. diameter). (e–h) Jet-milled and post-reheated samples (reheated at 750 °C for 3 h in air after milling): histograms of particle counts vs. diameter at grinding pressures of (e) 10 psi, (f) 60 psi, and (g) 120 psi; (h) corresponding cumulative distribution curves (percentage vs. diameter). Representative SEM images of the processed samples are provided in (i–n): (i) corresponding to (a), (j) corresponding to (b), (k) corresponding to (c), (l) corresponding to (e), (m) corresponding to (f), (n) corresponding to (g).

The influence of feed rate was then examined (**Figure 4, Table S2**). Three rates were tested: 0.1 g min^{-1}, 1.5 g min^{-1}, and 50 g min^{-1}, using the same 950 °C sintered NMC532 feedstock. At low to moderate feed rates (0.1 g min^{-1} and 1.5 g min^{-1}), jet milling produced uniform single-crystal particles with narrow particle size distribution and minimal agglomeration (**Figure 4a–b, 4i-j**). However, at 50 g min^{-1}, the particle size distribution broadened significantly, and residual agglomeration persisted (**Figure 4c–d, 4k**), indicating overload of the milling chamber and insufficient residence time for effective particle-on-particle collisions. An optimized feed rate is therefore required to balance processing efficiency, throughput, and product quality. SEM analysis of the re-heated samples (750 °C for 3 h) confirmed similar trends (**Figure 4e–h, 4l-n**): uniform, concentrated single crystal particles with narrow particle size distribution at 0.1 g min^{-1} and 1.5 g min^{-1}, but persistent agglomeration and broad particle size distribution at 50 g min^{-1}, highlighting the need for controlled restoring feed conditions to achieve sufficient deagglomeration.

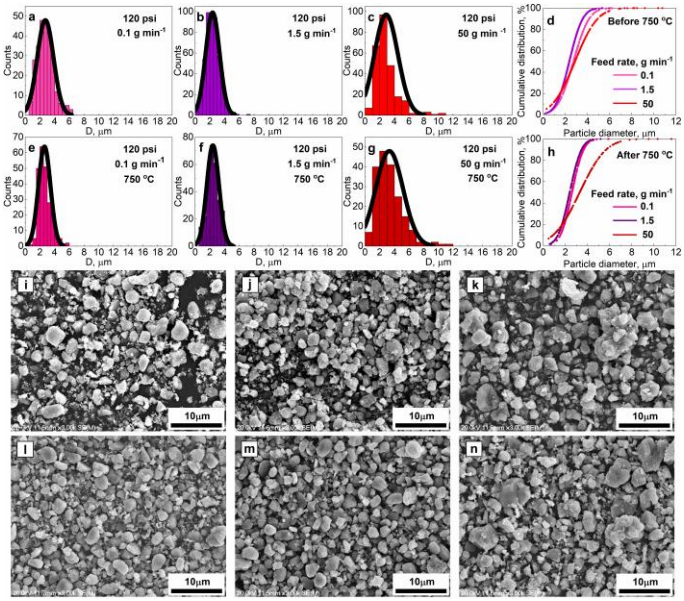

Figure 4. Particle size distributions of NMC532 cathode material determined from statistical SEM image analysis, showing the effect of feed rate in jet milling. (a–d) As-sintered NMC532 (one-pot all-dry synthesis at 950 °C for 10 h in air): histograms of particle counts vs. diameter at feed rate of (a) 0.1 g min^{-1}, (b) 1.5 g min^{-1}, and (c) 50 g min^{-1}; (d) corresponding cumulative distribution curves (percentage vs. diameter). (e–h) Jet-milled and post-reheated samples (reheated at 750 °C for 3 h in air after milling): histograms of particle counts vs. diameter at feed rate of (e) 0.1 g min^{-1}, (f) 1.5 g min^{-1}, and (g) 50 g min^{-1}; (h) corresponding cumulative distribution curves (percentage vs. diameter). Representative SEM images of the processed samples are provided in (i–n): (i) corresponding to (a), (j) corresponding to (b), (k) corresponding to (c), (l) corresponding to (e), (m) corresponding to (f), (n) corresponding to (g).

Although detailed electrochemical testing is beyond the scope of the present study, several expected implications of jet-milled particle morphology can be inferred from prior work on NMC cathodes. Processed homogeneous single crystal NMC is anticipated to exhibit excellent cycling performance by avoiding mechanical microcracking during cycling. For instance, single crystal NMC532 has demonstrated exceptional longevity, achieving more than 2500 cycles (>700 days of cycling) at C/3 and 55 °C when paired with an appropriate electrolyte[14]. In contrast, one-pot sintered NMC without proper de-agglomeration tends to display inferior rate capability and capacity retention. This inferior performance arises from the agglomeration of secondary particles, which lacks shortened lithium diffusion pathways[18].

Conclusions and Outlook

In conclusion, this study highlights jet milling as a powerful, enabling technology for all-dry LIB cathode materials manufacturing. By detailing the design, operating principles, and optimized protocols of a laboratory-scale fluid-energy mill, we address a key gap in the literature and provide practical guidance for the research community. In the case study, parametric investigations on all-dry synthesized single-crystal NMC532 demonstrate that grinding pressure (120 psi) and controlled feed rates (0.1–1.5 g min^{-1}) effectively deagglomerate sintered clusters into discrete, uniform primary particles (~3 µm) with narrow size distributions, preserved crystallinity, and improved morphological quality even after re-heating step.

Jet milling, as described by manufacturers and demonstrated in various applications, can achieve particle sizes down to approximately 100 nm (or even sub-100 nm), enabling the possibility of processing of LFP cathodes. Due to sluggish lithium-ion diffusion kinetics in olivine-structured LFP, nanoscale primary particles are critical to ensure good electrochemical performance and high rate capability, unlike NMC-based cathodes, which benefit from larger micron-sized (~3 µm) single crystals to optimize mechanical stability and minimize cracking during cycling. Furthermore, jet milling offers potential for dry surface coating of cathode materials. For instance, solid carbon precursors such as lignin can be mechanically mixed and coated onto cathode particles via high-velocity collisions in the jet mill, followed by inert-atmosphere heat treatment to form a uniform carbon layer that enhances electronic conductivity. Jet milling may also prove valuable for emerging materials, such as deagglomerating single crystal sodium layered oxide cathodes to achieve discrete primary particles.

All-dry battery materials production enabled by jet milling significantly reduces water and energy consumption, waste generation, and production costs compared with conventional aqueous routes. As global demand for rechargeable batteries surges to support electrification, scaling jet-milling systems, integrating real-

time monitoring, and validating full-cell performance will be critical next steps. These advancements promise more sustainable, scalable, and cost-effective battery manufacturing essential for the clean energy transition.

References

1. Safari A, Blaabjerg F, Oshnoei A. A research-industry perspective of battery systems technology for next-generation data centers. *J Energy Storage* 2026;152:120386. https://doi.org/10.1016/j.est.2026.120386.
2. Ngoy KR, Lukong VT, Yoro KO *et al*. Lithium-ion batteries and the future of sustainable energy: A comprehensive review. *Renewable and Sustainable Energy Reviews* 2025;223:115971. https://doi.org/10.1016/j.rser.2025.115971.
3. Xiao J, Cao X, Gridley B *et al*. From Mining to Manufacturing: Scientific Challenges and Opportunities behind Battery Production. *Chem Rev* 2025;125(13):6397–431. https://doi.org/10.1021/acs.chemrev.4c00980.
4. Zhang N, Yu H, Murphy A *et al*. A Liquid and Waste-free Method for Preparing Single Crystal Positive Electrode Materials for Li-ion Batteries. *J Electrochem Soc* 2023;170(7):070515. https://doi.org/10.1149/1945-7111/ace4f7.
5. Obrovac MN, Zheng L, Garayt MDL. Engineered Particle Synthesis by Dry Particle Microgranulation. *Cell Rep Phys Sci* 2020;1(6):100063. https://doi.org/10.1016/j.xcrp.2020.100063.
6. Guo Y, Zhang Q, Wei J *et al*. Advances and industrialization of $LiFePO_4$ cathodes in electric vehicles: challenges, innovations, and future directions. *J Mater Chem A Mater* 2025;13(23):17271–83. https://doi.org/10.1039/D5TA00166H.
7. Xiao J, Bi Y, Hwang S *et al*. Single Crystal Cathode Materials for Lithium-Based Batteries: Synthesis, Scaleup, and Manufacturing. *Chem Rev* 2025;125(22):11058–82. https://doi.org/10.1021/acs.chemrev.5c00485.
8. Shipitsyn V, Chak C (Michael), Jayakumar R *et al*. Revolutionizing Cathode Materials Processing: The Potential of Sustainable All Dry Methods. *Journal of Electrochemical Energy Conversion and Storage* 2026;23(2). https://doi.org/10.1115/1.4069378.
9. Nakach M, Authelin JR, Corsini C *et al*. Jet milling industrialization of sticky active pharmaceutical ingredient using quality-by-design approach. *Pharm Dev Technol* 2019;24(7):849–63. https://doi.org/10.1080/10837450.2019.1608449.
10. Urbaniak D, Otwinowski H, Wyleciał T *et al*. Research on the Grinding Energy Density in a Jet Mill. *Materials* 2021;14(8):2008. https://doi.org/10.3390/ma14082008.
11. Llorente A, Serrano B, Baselga J *et al*. Jet Milling as an Alternative Processing Technique for Preparing Polysulfone Hard Nanocomposites. *Advances in Materials Science and Engineering* 2019;2019:1–8. https://doi.org/10.1155/2019/3501402.
12. Angelidis G, Protonotariou S, Mandala I *et al*. Jet milling effect on wheat flour characteristics and starch hydrolysis. *J Food Sci Technol* 2016;53(1):784–91. https://doi.org/10.1007/s13197-015-1990-1.
13. Yu S, Zhang N, Garayt M *et al*. All dry in one step (ADIOS to water) synthesis of W-coated $Li_{1+x}(Ni_{0.7}Mn_{0.3})_{1-x}O_2$. *J Power Sources* 2023;581:233432. https://doi.org/10.1016/j.jpowsour.2023.233432.
14. Harlow JE, Ma X, Li J *et al*. A Wide Range of Testing Results on an Excellent Lithium-Ion Cell Chemistry to be used as Benchmarks for New Battery Technologies. *J Electrochem Soc* 2019;166(13):A3031–44. https://doi.org/10.1149/2.0981913jes.
15. Choi J, Dong L, Yu CY *et al*. Relationship of Chemical Composition and Moisture Sensitivity in $LiNi_xMn_yCo_{1-x-y}O_2$ for Lithium-Ion Batteries. *Journal of Electrochemical Energy Conversion and Storage* 2021;18(4). https://doi.org/10.1115/1.4051208.
16. Winkowska-Struzik M, Buchberger DA, Uhrynowski W *et al*. Air Storage Impact on Surface Evolution of Stoichiometric and Li-Rich NMC811. *ACS Omega* 2024;9(51):50334–48. https://doi.org/10.1021/acsomega.4c06636.
17. Bichon M, Sotta D, Dupré N *et al*. Study of Immersion of $LiNi_{0.5}Mn_{0.3}Co_{0.2}O_2$ Material in Water for Aqueous Processing of Positive Electrode for Li-Ion Batteries. *ACS Appl Mater Interfaces* 2019;11(20):18331–41. https://doi.org/10.1021/acsami.9b00999.
18. Laurie Carrier, M. N. Obrovac, In Situ Deagglomeration of Cathode Particles in Electrode Slurries. *J Electrochem Soc* 2025;172:050506. 10.1149/1945-7111/add095.